

DDT: Dual-branch Deformable Transformer for Image Denoising

Kangliang Liu¹, Xiangcheng Du^{1,2}, Sijie Liu¹, Yingbin Zheng², Xingjiao Wu¹, Cheng Jin^{1*}

¹*School of Computer Science, Fudan University, Shanghai, China* ²*Videt Technology, Shanghai, China*

{klliu21, xcd22, sjliu22}@m.fudan.edu.cn, zyb@videt.cn, {xjwu_cs, jc}@fudan.edu.cn

Abstract—Transformer is beneficial for image denoising tasks since it can model long-range dependencies to overcome the limitations presented by inductive convolutional biases. However, directly applying the transformer structure to remove noise is challenging because its complexity grows quadratically with the spatial resolution. In this paper, we propose an efficient Dual-branch Deformable Transformer (DDT) denoising network which captures both local and global interactions in parallel. We divide features with a fixed patch size and a fixed number of patches in local and global branches, respectively. In addition, we apply deformable attention operation in both branches, which helps the network focus on more important regions and further reduces computational complexity. We conduct extensive experiments on real-world and synthetic denoising tasks, and the proposed DDT achieves state-of-the-art performance with significantly fewer computational costs. The source code and trained models are available at <https://github.com/Merenguelk/DDT>.

Index Terms—Image denoising, dual-branch, transformer, deformable attention

I. INTRODUCTION

Image denoising is a foundational task of low-level vision, which aims to remove unwanted noise signals from input images and recover noise-free clean images. The task is widely used as a pre-processing technique for many high-level vision applications, such as image classification, object detection, and semantic segmentation.

Traditional methods leverage image priors to solve the degradation problem [1], [2]. However, these methods are highly dependent on hand-crafted features and are time-consuming, which limits applications in real-world scenarios. Recently, CNN-based denoising methods [3], [4] have achieved remarkable performance. Although convolutional operation provides inductive bias of local connectivity and translation equivariance, the limited receptive field hinders modeling long-range dependencies over a whole image.

Inspired by the astounding performance of Transformer models in NLP field [6], research has moved towards applying the same principles in computer vision [7]–[9]. The feature representations generated from self-attention components do not contain the spatial constraints imposed by convolutional operations. However, the standard self-attention suffers from quadratic complexity with the length of sequences, making it hard to apply to the pixel level directly.

To solve these problems, some low-level Transformer models [10]–[12] utilize local or channel-wise attention but not

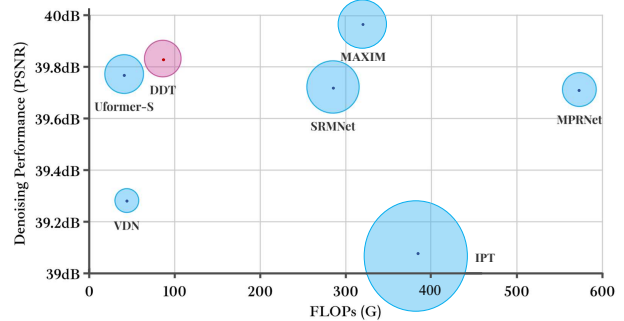


Fig. 1. Denoising results (PSNR) *vs.* computational cost (FLOPs) on SIDD dataset [5]. The radius of circle represents the number of parameters.

fully exploiting the global modeling advantage of the Transformer. We consider local and global information equally useful for image denoising, so we use a parallel structure to process both of them efficiently. Besides, highly similar patterns often appear repeatedly, and it is redundant to calculate all these regions. Therefore, we propose an adaptively deformable operation to reduce these redundant calculations while focusing on more informative areas.

In this paper, we propose an effective Dual-branch Deformable Transformer (DDT) network for image denoising. DDT applies parallelly local and global branches with the deformable attention strategy. Specifically, we first divide the input feature into patches using different rules in both branches, then perform deformable attention inside patches in the local branch and among the same relative locations of each patch in the global branch. In the deformable attention, we reduce the number of key-value pairs, preserving more informative ones adaptively and saving calculational costs furtherly. In this way, global receptive fields and local aggregations are both involved in our Transformer model with linear complexity by the dual-branch structure, and the deformable attention mechanism also reduces redundant calculations. The main contributions of our work are summarized as follows:

- We propose an efficient Dual-branch Deformable Transformer denoising network that can process high-resolution noisy images in linear complexity.
- Deformable attention is introduced to reduce redundant calculations and focus on more informative regions.
- Extensive experiments prove that our method can produce more competitive performance with fewer computational costs than other state-of-the-art methods.

*Corresponding author.

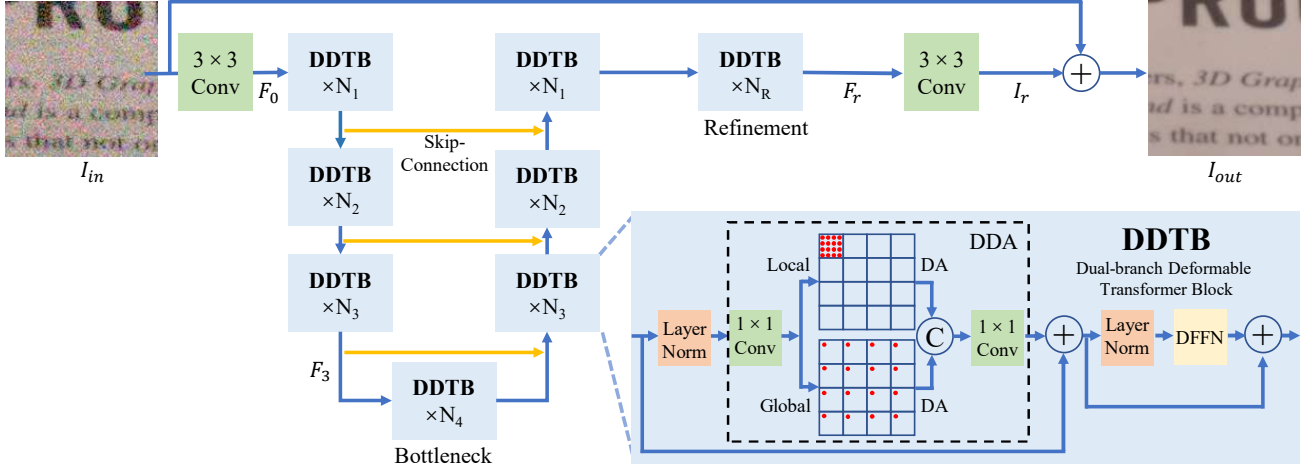


Fig. 2. The overall architecture of the Dual-branch Deformable Transformer. The Unet-like hierarchical architecture with an extra refinement stage is used for image denoising, and each stage contains a different number of Dual-branch Deformable Transformer Blocks (DDTBs). The DDTB captures the local and global features parallelly using Dual-branch Deformable Attention (DDA) and Depth-wise Feed-Forward Network (DFFN).

II. RELATED WORK

A. Image Denoising

Image denoising, as a fundamental low-level task, has been studied for decades. Traditional methods usually leverage image priors and handcrafted features. The representative block-matching 3D (BM3D) [13] utilizes the nonlocal similarity and transform-domain technique and follows three consecutive stages: grouping, collaborative filtering, and aggregation.

With the development of deep learning, many learning-based denoising methods have been proposed and achieved remarkable performance. GCBD [14] introduces GAN [15] to image denoising tasks. GCDN [16] captures self-similar information for denoising. FFDNet [17] takes a tunable noise level map as input and enhances flexibility to deal with spatially variant noise. MPRNet [4] uses a multi-stage architecture to achieve state-of-the-art. Besides, some works try to extract global features to improve denoising results. MAXIM [18] explores the potential of MLP in image restoration, and others [10]–[12], [19] utilize attention mechanisms [6] for global modeling. However, these methods have characteristics of high memory occupation and time consumption.

B. Vision Transformer

Transformer structure was first proposed for natural language processing tasks [6] with multi-head self-attention. Recently, the Vision Transformer (ViT) [7] has surpassed previous state-of-the-art CNN-based models on the image classification task by projecting image patches into sequences and feeding them to Transformer blocks. PVT [9] uses a pyramid architecture to leverage multi-scale features and improves performance on object detection and instance segmentation tasks. Swin-Transformer [8] proposes shifted window-based attention mechanism, reducing the computational cost compared with ViT. Reference [20], [21] introduce a deformable strategy to reduce the number of key-value pairs in Transformer.

Inspired by the long-range dependencies modeling ability of Vision Transformers, researchers also exhibit its potential in low-level tasks. IPT [19] proposes a pre-trained backbone for image restoration. In order to reduce high computational complexity, SwinIR [11] and Uformer [10] apply attention in local windows with shifted window operation. Restormer [12] leverages attention on channel dimension as a global operation, avoiding huge calculation costs on spatial level but lacking locality. Different from previous works, our novel framework DDT can leverage both local and global contexts effectively and demonstrates high efficiency.

III. APPROACH

Our main purpose is to develop an efficient Transformer model that can process high-resolution images for the image denoising tasks. In order to enhance feature representations, we use a dual-branch structure to parallelly capture local and global features. In addition, we use a deformable strategy to focus attention on more important regions and further reduce computational costs. The overall pipeline of the Dual-branch Deformable Transformer is described as Fig. 2.

A. Overall Pipeline

Given a noisy image $I_{in} \in \mathbb{R}^{H \times W \times 3}$, the input is first projected into the feature $F_0 \in \mathbb{R}^{H \times W \times C}$ by a 3×3 convolution layer. Then the feature F_0 goes through a 4-stage Unet-like encoder-decoder architecture. Each stage includes multiple DDTBs and a sample layer (*i.e.* downsample or upsample). The output feature $F_3 \in \mathbb{R}^{\frac{H}{8} \times \frac{W}{8} \times 8C}$ goes through the Bottleneck and is fed into the decoder. The decoder has a symmetrical structure, where an upsample layer is used at the beginning of each stage. The skip-connection [22] is used to boost performance, and we use the concatenation operation and a 1×1 convolution layer for feature fusion. Inspired by [12], we introduce a refinement stage after the decoder, which aims to enhance feature representation for more details.

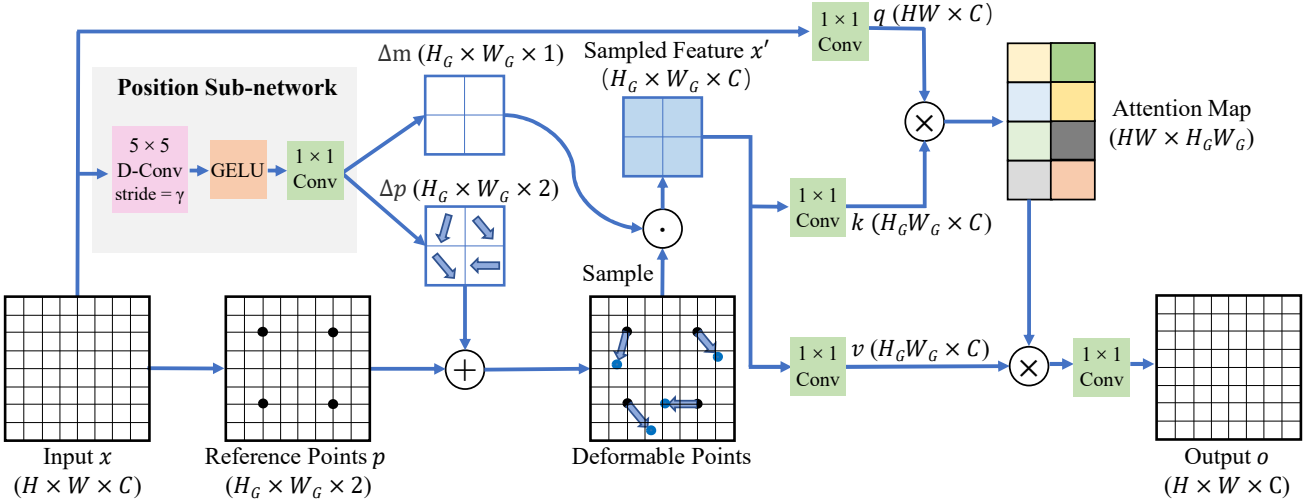


Fig. 3. The structure of deformable attention. A group of offsets Δp are learned from the input x and added on the pre-defined reference points p to get deformable points. Features x' sampled from the input at the positions of deformable points are then projected as keys(k) and values(v), while queries(q) are still from the input x .

of images. Finally, the feature F_r from the refinement stage through a 3×3 convolution filter to obtain the residual image $I_r \in \mathbb{R}^{H \times W \times 3}$, and the restored output I_{out} is denoted as:

$$I_{out} = I_{in} + I_r \quad (1)$$

B. Dual-branch Deformable Transformer Block

DDTB consists of two main components: Dual-branch Deformable Attention (DDA) and Depth Feed-Forward Network (DFFN). A layer normalization is first applied in each part. Specifically, DDA splits the feature over the channel dimension and sends them into a dual-branch structure, where local and global interactions are performed parallelly. In the local branch, we divide the feature into non-overlapping patches with pre-defined patch sizes and apply the spatial attention mechanism inside the patches. In the global branch, we use a pre-defined number of patches to do the patch partitioning and perform calculations among the corresponding positions of each patch. The multi-scale features output by the dual-branch are then fused by concatenation operation and a linear layer. We utilize a deformable attention mechanism as the spatial operation in both branches, which will be introduced in Section III-C.

Inspired by [12], [23], we add depth-wise convolution into the standard Feed-Forward Network [7] as DFFN to further enhance features. Formally, The l -th DDTB is formulated as:

$$\hat{X}_l = \text{DDA}(\text{LN}(X_{l-1})) + X_{l-1} \quad (2)$$

$$X_l = \text{DFFN}(\text{LN}(\hat{X}_l)) + \hat{X}_l \quad (3)$$

where X_{l-1} represents the output of $(l-1)$ th DDTB, and LN means the layer normalization. The residual connection [24] is used in both components. With the dual-branch structure, we can process inputs with linear complexity, making it possible to process high-resolution images using Transformer architecture, preserving global receptive fields while capturing locality.

C. Deformable Attention

To further save computational costs, the deformable attention (Fig. 3) is applied for efficient spatial operation. Inspired by [21], we first define a set of grid-shape reference points $p \in \mathbb{R}^{H_G \times W_G \times 2}$ based on the input $x \in \mathbb{R}^{H \times W \times C}$. The number of points is determined by a hyper-parameter γ , $H_G = H/\gamma$ and $W_G = W/\gamma$. Meanwhile, we feed x into a Position Sub-network containing a 5×5 depth-wise convolutional layer with stride γ . The output of the sub-network has three channels, and the first two channels are deformable offsets $\Delta p \in \mathbb{R}^{H_G \times W_G \times 2}$ for each reference point. We add the offsets Δp on each point to obtain the deformable points and sample the feature $x' \in \mathbb{R}^{H_G \times W_G \times C}$ from x . The remaining channel is used as a modulation scalar $\Delta m \in \mathbb{R}^{H_G \times W_G \times 1}$ to multiply x' , aiming to enhance the spatial representations. The sampled feature x' can be expressed as:

$$x' = \psi(x, p + \Delta p) \odot \Delta m \quad (4)$$

where \odot denotes element-wise multiplication, and $\psi(\cdot, \cdot)$ represents the sampling process. We leverage bilinear interpolation to make this process differentiable.

Then we apply linear projections on x and x' to obtain queries(q), keys(k) and values(v) and perform multi-head attention with M heads to get the output o :

$$q = W_q x, k = W_k x', v = W_v x' \quad (5)$$

$$z^{(m)} = \text{softmax}\left(\frac{q^{(m)} k^{(m)\top}}{\sqrt{d}}\right) v^{(m)}, m = 1, 2, \dots, M \quad (6)$$

$$o = W_o \text{concat}(z^{(1)}, z^{(2)}, \dots, z^{(M)}) \quad (7)$$

where $W_{(\cdot)} \in \mathbb{R}^{C \times C}$ is the 1×1 convolution for linear projection, and $d = C/M$ is the number of channels for each head. $z^{(m)}, q^{(m)}, k^{(m)}, v^{(m)}$ represent the output, queries, keys and values in the m -th head. It is noteworthy that k and v are

generated from the sampled feature x' with size $H_G W_G \times C$, which is smaller than q .

We consider that the sampled feature x' preserves most of the important information of x , reducing redundant contents compared with the origin feature x . It is a data-dependent way that can adapt to different inputs. In this way, we reduce the computation on redundant areas and let the model focus on more informative regions.

D. Analysis of Computational Cost

Our method consists of DDTBs with different scales. The computational costs of DDTB come mainly from Dual-branch Deformable Attention (DDA), which consists of two convolutional layers and a dual-branch structure. We assume the input size for DDA as $H \times W \times C$, and the patch size and the number of patch in the local and global branches as $p \times p$ equally.

Convolutional layers. There are two 1×1 convolutional layers in DDA for channel expanding and feature fusion, respectively. We denote each of them as:

$$\Omega(\text{Conv}) = 2HWC^2 \quad (8)$$

Dual-branch structure. The deformable attention (DA) is applied in the local and global branches. We take the local branch as an example to illustrate the computational costs. We first divide the input into patches with size $p \times p \times C$, so we get HW/p^2 patches. We feed them into DA for local feature extraction. The hyper-parameter in DA for controlling the number of keys and values is γ . We take each branch's costs as:

$$\Omega(\text{Branch}) = \frac{2\gamma^2 + 2}{\gamma^2} HWC^2 + \frac{2p^2 + 29}{\gamma^2} HWC + \frac{2}{\gamma^2} HW \quad (9)$$

The global branch divides the input into $p \times p$ patches and perform DA among the corresponding positions of each patch, the costs of which are same as equation (9).

Overall, we present the computational costs of DDA as:

$$\begin{aligned} \Omega(\text{DDA}) &= 2\Omega(\text{Conv}) + 2\Omega(\text{Branch}) \\ &= \frac{8\gamma^2 + 4}{\gamma^2} HWC^2 + \frac{4p^2 + 58}{\gamma^2} HWC + \frac{4}{\gamma^2} HW \end{aligned} \quad (10)$$

where the computational costs are linear with the spatial resolution HW , indicating that it is possible to apply the proposed DDT on high-resolution images frequently appearing in image denoising tasks.

IV. EXPERIMENTS

In this section, we first introduce datasets and implementation details. Next, we describe extensive comparisons with previous methods. Moreover, we perform ablation studies to evaluate the effectiveness of each component.

TABLE I
THE QUANTITATIVE RESULTS OF REAL-WORLD DENOISING ON SIDD AND DND DATASETS. THE BOLD NUMBERS REPRESENT THE BEST RESULTS. F AND P DENOTE FLOPS AND PARAMETERS, RESPECTIVELY.

Method	F(G)	P(M)	SIDD [5]		DND [25]	
			PSNR	SSIM	PSNR	SSIM
Restormer [12]	155	26.1	40.02	0.960	40.03	0.956
MAXIM [18]	339	22.2	39.96	0.960	39.84	0.954
Uformer-B [10]	86	50.9	39.89	0.960	40.04	0.956
SRMNet [32]	285	37.6	39.72	0.959	39.44	0.951
MIRNet [33]	785	31.8	39.72	0.959	39.88	0.956
MPRNet [4]	573	15.7	39.71	0.958	39.80	0.954
CycleISP* [34]	184	2.8	39.52	0.957	39.56	0.956
DANet [35]	30	63.0	39.30	0.916	39.59	0.955
VDN [36]	44	7.8	39.28	0.909	39.38	0.952
IPT* [19]	380	115.3	39.10	0.954	39.62	0.952
RIDNet* [37]	98	1.5	38.71	0.914	39.26	0.953
DDT (ours)	86	18.4	39.83	0.960	39.78	0.954

* denotes methods using additional training data.

A. Datasets

Real-world denoising. For real-world denoising, we train DDT on the SIDD [5] training set and test on both SIDD validation set and DND online benchmark [25]. SIDD provides noisy-clean image pairs from 10 scenes under different lighting conditions using five representative smartphone cameras. DND is an online benchmark of 50 image pairs captured with four consumer cameras.

Synthetic denoising. We add Gaussian noise to some natural image datasets [26], [27] with random sigma ranging from [0, 50] to generate noisy-clean image pairs for training. We select Gaussian noise with sigma 15, 25, and 50 on datasets CBSD68 [28], Kodak24 [29], McMaster [30] and Urban100 [31] as testsets.

B. Implementation Details

DDT adopts a 4-stage encoder-decoder architecture. Following [12], we set the number of DDTBs from the 1st stage to Bottleneck as (4, 6, 6, 8) with the number of attention heads (1, 2, 4, 8) and 4 extra blocks for the Refinement stage. The channel number in the 1st stage is set as 32, which will increase gradually in deeper stages. We use AdamW [41] optimizer ($\beta_1 = 0.9$, $\beta_2 = 0.99$, weight decay $1e^{-4}$) and L_1 loss with 300K iterations for optimization. The learning rate is initialized as $3e^{-4}$ and reduce to $1e^{-6}$ with the cosine annealing scheduler [42]. Progressive learning strategy [12] from 128×128 to 256×256 is also used, and we utilize rotation and flips for data augmentations. All training processes are conducted on 4 NVIDIA TITAN Xp GPUs.

C. Comparison with State-of-the-arts

Real-world denoising. Table I reports the real-world denoising results on the SIDD and DND datasets. We compare DDT with state-of-the-art methods, including CNN-based, MLP-based and Transformer-based methods. Our proposed DDT achieves competitive performance on the SIDD dataset, getting state-of-the-art results on SSIM with the fewest parameters and FLOPs. MAXIM [18] and Restormer [12] surpass our DDT by

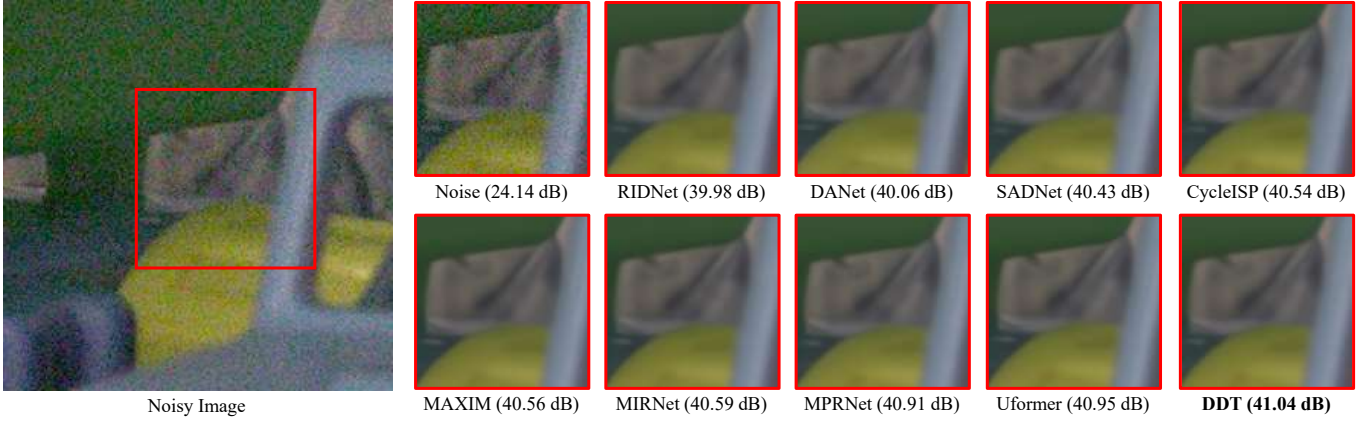


Fig. 4. Visual comparisons with state-of-the-art methods on real-world image denoising.

TABLE II
COMPARISON RESULTS OF SYNTHETIC DENOISING. THE **BOLD** AND UNDERLINE REPRESENT THE BEST AND THE SECND BEST RESULTS.

Method	F(G)	P(M)	CBSD68 [28]			Kodak24 [29]			McMaster [30]			Urban100 [31]		
			$\sigma=15$	$\sigma=25$	$\sigma=50$	$\sigma=15$	$\sigma=25$	$\sigma=50$	$\sigma=15$	$\sigma=25$	$\sigma=50$	$\sigma=15$	$\sigma=25$	$\sigma=50$
IRCNN [38]	49	0.7	33.86	31.16	27.86	34.69	32.18	28.93	34.58	32.18	28.91	33.78	31.20	27.70
DnCNN [3]	93	1.4	33.94	31.30	28.02	34.64	32.14	28.99	34.69	32.32	38.23	33.80	31.34	27.98
DSNet [39]	-	-	33.91	31.28	28.05	34.63	32.16	29.05	34.67	32.40	29.28	-	-	-
MLEFGN [40]	447	6.9	-	-	28.21	-	-	29.38	-	-	-	-	-	28.92
IPT [19]	380	115.3	-	-	28.39	-	-	29.64	-	-	29.98	-	-	<u>29.71</u>
Restormer [12]	155	26.1	34.39	31.78	28.59	<u>35.44</u>	<u>33.02</u>	<u>30.00</u>	35.55	33.31	30.29	35.06	32.91	30.02
DDT (ours)	86	18.4	<u>34.30</u>	<u>31.69</u>	<u>28.50</u>	<u>35.31</u>	<u>32.88</u>	<u>29.85</u>	<u>35.36</u>	<u>33.11</u>	<u>30.07</u>	<u>34.80</u>	<u>32.58</u>	29.56

0.13dB and 0.19dB on PSNR, but ours only takes 25.4% and 55.5% FLOPs compared to them respectively, demonstrating the efficiency of DDT. Uformer-B uses 50.9M parameters and gets better results, but our DDT performs better when Uformer-S uses a similar number of parameters. To show results more clearly, we present the PSNR vs. FLOPs in Fig. 1, in which the radius of each point represents the number of parameters. We also show the visual results with various state-of-the-art methods on SIDD in Fig. 4, and it is obviously observed that DDT not only removes noise but preserves sharp and clear details.

Synthetic denoising. Table II shows PSNR values of different methods for synthetic denoising. We select various methods using consistent experiment settings for comparison, including IRCNN [38], DnCNN [3], DSNet [39], MLEFGN [40], IPT [19] and Restormer [12]. DDT efficiently achieves suboptimal performance only lower than Restormer, but Restormer takes 1.8x more computational costs. Our results surpass another Transformer model IPT on CBSD68, Kodak24 and McMaster datasets, which uses 6.26× more parameters and 4.42× more FLOPs compared with our DDT.

D. Ablation Studies

In this section, we conduct ablation studies to evaluate the performance of the dual-branch structure and deformable attention on the SIDD dataset.

TABLE III
EFFECTS OF DUAL-BRANCH STRUCTURE.

Local	Global	PSNR	F (G)	P (M)
✓		39.77	86	18.4
	✓	39.78	86	18.4
✓	✓	39.83	86	18.4

TABLE IV
COMPARISON WITH DIFFERENT SPATIAL OPERATIONS.

Operation	PSNR	F (G)	P (M)
MLP	39.65	121	18.4
MHSA	39.76	157	18.3
DA (ours)	39.83	86	18.4

Dual-branch. To evaluate the effectiveness of dual-branch structure, we conduct experiments with a single branch (*i.e.* only using local or global branch). For a fair comparison, we double the number of channels when using a single branch to keep the same parameters as the dual-branch's. The results are shown in Table III. We observed similar results when using a single branch. However, by combining them into the parallelly dual-branch structure, the PSNR improved by 0.06dB and 0.05dB, respectively.

Deformable attention. Deformable attention reduces redundant computations and focuses on more important regions. We compared with multilayer perceptron (MLP) and standard multi-head self-attention (MHSA) [7] which have quadratic

complexity to show our deformable attention's effectiveness and high efficiency. We adjust the number of layers in MLP and the number of channels in MHSA to maintain a similar number of parameters (~ 18.4 M). Table IV shows the detailed results that our deformable attention achieves the best performance with only 71.1% and 54.8% computational costs of MLP and MHSA.

V. CONCLUSIONS

In this paper, we present an efficient and effective Transformer model DDT for image denoising, which is computationally efficient for processing high-resolution images. Specifically, we use a dual-branch structure in Dual-branch Deformable Transformer Blocks, parallel modeling local and global information with linear complexity. To further save computational resources, deformable attention is also applied, reducing redundant calculations and focusing on more informative regions. Experimental results on synthetic and real-world denoising tasks demonstrate that our method achieves competitive results using a small number of computations.

REFERENCES

- [1] M. Elad and M. Aharon, "Image denoising via sparse and redundant representations over learned dictionaries," *IEEE Transaction on Image Processing*, vol. 15, no. 12, pp. 3736–3745, 2006.
- [2] L. I. Rudin, S. Osher, and E. Fatemi, "Nonlinear total variation based noise removal algorithms," *Physica D: nonlinear phenomena*, vol. 60, no. 1-4, pp. 259–268, 1992.
- [3] K. Zhang, W. Zuo, Y. Chen, D. Meng, and L. Zhang, "Beyond a gaussian denoiser: Residual learning of deep cnn for image denoising," *IEEE Transaction on Image Processing*, vol. 26, no. 7, pp. 3142–3155, 2017.
- [4] S. W. Zamir, A. Arora, S. Khan, M. Hayat, F. S. Khan, M.-H. Yang, and L. Shao, "Multi-stage progressive image restoration," in *CVPR*, 2021, pp. 14821–14831.
- [5] A. Abdelhamed, S. Lin, and M. S. Brown, "A high-quality denoising dataset for smartphone cameras," in *CVPR*, 2018, pp. 1692–1700.
- [6] A. Vaswani, N. Shazeer, N. Parmar, J. Uszkoreit, L. Jones, A. N. Gomez, Ł. Kaiser, and I. Polosukhin, "Attention is all you need," *NeurIPS*, 2017.
- [7] A. Dosovitskiy, L. Beyer, A. Kolesnikov, D. Weissenborn, X. Zhai, T. Unterthiner, M. Dehghani, M. Minderer, G. Heigold, S. Gelly, et al., "An image is worth 16x16 words: Transformers for image recognition at scale," *arXiv:2010.11929*, 2020.
- [8] Z. Liu, Y. Lin, Y. Cao, H. Hu, Y. Wei, Z. Zhang, S. Lin, and B. Guo, "Swin transformer: Hierarchical vision transformer using shifted windows," in *ICCV*, 2021, pp. 10012–10022.
- [9] W. Wang, E. Xie, X. Li, D.-P. Fan, K. Song, D. Liang, T. Lu, P. Luo, and L. Shao, "Pyramid vision transformer: A versatile backbone for dense prediction without convolutions," in *ICCV*, 2021, pp. 568–578.
- [10] Z. Wang, X. Cun, J. Bao, W. Zhou, J. Liu, and H. Li, "Uformer: A general u-shaped transformer for image restoration," in *CVPR*, 2022, pp. 17683–17693.
- [11] J. Liang, J. Cao, G. Sun, K. Zhang, L. Van Gool, and R. Timofte, "Swinir: Image restoration using swin transformer," in *ICCV*, 2021, pp. 1833–1844.
- [12] S. W. Zamir, A. Arora, S. Khan, M. Hayat, F. S. Khan, and M.-H. Yang, "Restormer: Efficient transformer for high-resolution image restoration," in *CVPR*, 2022, pp. 5728–5739.
- [13] K. Dabov, A. Foi, V. Katkovnik, and K. Egiazarian, "Image denoising by sparse 3-d transform-domain collaborative filtering," *IEEE Transaction on Image Processing*, vol. 16, no. 8, pp. 2080–2095, 2007.
- [14] J. Chen, J. Chen, H. Chao, and M. Yang, "Image blind denoising with generative adversarial network based noise modeling," in *CVPR*, 2018, pp. 3155–3164.
- [15] A. Radford, L. Metz, and S. Chintala, "Unsupervised representation learning with deep convolutional generative adversarial networks," *arXiv:1511.06434*, 2015.
- [16] D. Valsesia, G. Fracastoro, and E. Magli, "Deep graph-convolutional image denoising," *IEEE Transaction on Image Processing*, vol. 29, pp. 8226–8237, 2020.
- [17] K. Zhang, W. Zuo, and L. Zhang, "Ffdnet: Toward a fast and flexible solution for cnn-based image denoising," *IEEE Transaction on Image Processing*, vol. 27, no. 9, pp. 4608–4622, 2018.
- [18] Z. Tu, H. Talebi, H. Zhang, F. Yang, P. Milanfar, A. Bovik, and Y. Li, "Maxim: Multi-axis mlp for image processing," in *CVPR*, 2022, pp. 5769–5780.
- [19] H. Chen, Y. Wang, T. Guo, C. Xu, Y. Deng, Z. Liu, S. Ma, C. Xu, C. Xu, and W. Gao, "Pre-trained image processing transformer," in *CVPR*, 2021, pp. 12299–12310.
- [20] X. Zhu, W. Su, L. Lu, B. Li, X. Wang, and J. Dai, "Deformable detr: Deformable transformers for end-to-end object detection," *arXiv:2010.04159*, 2020.
- [21] Z. Xia, X. Pan, S. Song, L. E. Li, and G. Huang, "Vision transformer with deformable attention," in *CVPR*, 2022, pp. 4794–4803.
- [22] O. Ronneberger, P. Fischer, and T. Brox, "U-net: Convolutional networks for biomedical image segmentation," in *MICCAI*, 2015, pp. 234–241.
- [23] H. Lee, H. Choi, K. Sohn, and D. Min, "Knn local attention for image restoration," in *CVPR*, 2022, pp. 2139–2149.
- [24] K. He, X. Zhang, S. Ren, and J. Sun, "Deep residual learning for image recognition," in *CVPR*, 2016, pp. 770–778.
- [25] T. Plotz and S. Roth, "Benchmarking denoising algorithms with real photographs," in *CVPR*, 2017, pp. 1586–1595.
- [26] E. Agustsson and R. Timofte, "Ntire 2017 challenge on single image super-resolution: Dataset and study," in *CVPR Workshops*, 2017, pp. 126–135.
- [27] R. Timofte, E. Agustsson, L. Van Gool, M.-H. Yang, and L. Zhang, "Ntire 2017 challenge on single image super-resolution: Methods and results," in *CVPR Workshops*, 2017, pp. 114–125.
- [28] D. Martin, C. Fowlkes, D. Tal, and J. Malik, "A database of human segmented natural images and its application to evaluating segmentation algorithms and measuring ecological statistics," in *ICCV*, 2001, pp. 416–423.
- [29] R. Franzen, "Kodak lossless true color image suite," in <http://r0k.us/graphics/kodak/>, 1999.
- [30] L. Zhang, X. Wu, A. Buades, and X. Li, "Color demosaicking by local directional interpolation and nonlocal adaptive thresholding," *Journal of Electronic Imaging*, vol. 20, no. 2, pp. 023016, 2011.
- [31] J.-B. Huang, A. Singh, and N. Ahuja, "Single image super-resolution from transformed self-exemplars," in *CVPR*, 2015, pp. 5197–5206.
- [32] C.-M. Fan, T.-J. Liu, K.-H. Liu, and C.-H. Chiu, "Selective residual net for real image denoising," in *EUSIPCO*, IEEE, 2022, pp. 469–473.
- [33] S. W. Zamir, A. Arora, S. Khan, M. Hayat, F. S. Khan, M.-H. Yang, and L. Shao, "Learning enriched features for real image restoration and enhancement," in *ECCV*, 2020, pp. 492–511.
- [34] S. W. Zamir, A. Arora, S. Khan, M. Hayat, F. S. Khan, M.-H. Yang, and L. Shao, "Cycleisp: Real image restoration via improved data synthesis," in *CVPR*, 2020, pp. 2696–2705.
- [35] Z. Yue, Q. Zhao, L. Zhang, and D. Meng, "Dual adversarial network: Toward real-world noise removal and noise generation," in *ECCV*. Springer, 2020, pp. 41–58.
- [36] Z. Yue, H. Yong, Q. Zhao, D. Meng, and L. Zhang, "Variational denoising network: Toward blind noise modeling and removal," *NeurIPS*, vol. 32, 2019.
- [37] S. Anwar and N. Barnes, "Real image denoising with feature attention," in *ICCV*, 2019, pp. 3155–3164.
- [38] K. Zhang, W. Zuo, S. Gu, and L. Zhang, "Learning deep cnn denoiser prior for image restoration," in *CVPR*, 2017, pp. 3929–3938.
- [39] Y. Peng, L. Zhang, S. Liu, X. Wu, Y. Zhang, and X. Wang, "Dilated residual networks with symmetric skip connection for image denoising," *Neurocomputing*, vol. 345, pp. 67–76, 2019.
- [40] F. Fang, J. Li, Y. Yuan, T. Zeng, and G. Zhang, "Multilevel edge features guided network for image denoising," *IEEE Transactions on Neural Networks and Learning Systems*, vol. 32, no. 9, pp. 3956–3970, 2020.
- [41] I. Loshchilov and F. Hutter, "Decoupled weight decay regularization," *arXiv:1711.05101*, 2017.
- [42] I. Loshchilov and F. Hutter, "Sgdr: Stochastic gradient descent with warm restarts," *arXiv:1608.03983*, 2016.

APPENDIX

In this appendix, We will show the derivation process of the equations in Section 3.4.

A. Deformable Attention

Assuming the input feature size to the deformable attention (DA) is $H \times W \times C$, and the stride in DA's Position Sub-network is γ . We divide the computations of DA into four parts: Position Sub-network, Convolutional layers, Δp and Δm , and multi-head attention.

Position sub-network. There is a 5×5 depth-wise convolutional layer with stride γ and a 1×1 convolutional layer to reduce the number of channel to 3. Therefore, we can summarize the Position Sub-network (PS)'s computational costs as:

$$\Omega(\text{PS}) = 5^2 \cdot \frac{HW}{r^2} C + 3 \cdot \frac{HW}{r^2} C \quad (11)$$

Convolutional layers. There are four 1×1 convolutional layers for generating q , k , v and o . Based on the different input sizes, we denote their costs as:

$$\Omega(q) = HWC^2 \quad (12)$$

$$\Omega(k) = \frac{HW}{r^2} C^2 \quad (13)$$

$$\Omega(v) = \frac{HW}{r^2} C^2 \quad (14)$$

$$\Omega(o) = HWC^2 \quad (15)$$

Δp and Δm . The Δp and Δm output by the Position Sub-network are then element-wise added on the reference points and element-wise multiplied on the sampled feature, respectively. We express their costs as:

$$\Omega(\Delta p) = 2 \cdot \frac{HW}{r^2} \quad (16)$$

$$\Omega(\Delta m) = \frac{HW}{r^2} C \quad (17)$$

Multi-head attention. After obtaining q , k and v , Multi-head attention (MHA) is applied. there existing 2 matrix multiplications among q , k , v .

$$\Omega(\text{MHA}) = 2 \cdot \frac{H^2 W^2}{r^2} C \quad (18)$$

We summarize the overall computational costs of the deformable attention (DA) by adding up Equation (11) - (18) as:

$$\begin{aligned} \Omega(\text{DA}) = & \frac{2}{\gamma^2} H^2 W^2 C + \left(2 + \frac{2}{\gamma^2}\right) HWC^2 \\ & + \frac{29}{\gamma^2} HWC + \frac{2}{\gamma^2} HW \end{aligned} \quad (19)$$

B. Dual-branch Deformable Attention

Dual-branch Deformable Attention (DDA) consists of two 1×1 convolutional layers and a dual-branch structure. We assume the input size for DDA as $H \times W \times C$, and the patch size and the number of patch in the local and global branches as $p \times p$ equally.

Convolutional layers. There are two 1×1 convolutional layers in DDA. One is used for expanding channels before the dual-branch structure, and the other for multi-scale features fusion after the dual-branch. We denote each of them as:

$$\Omega(\text{Conv}) = 2HWC^2 \quad (20)$$

Local and global branch. The DA is applied inside and among the patches in the local and global branches, respectively. We take the local branch as an example to illustrate the computational costs. We first divide the input into patches with size $p \times p \times C$, so we get HW/p^2 patches. We feed them into DA for local feature extraction. We take the patch size into equation (19) to get one branch's costs as:

$$\begin{aligned} \Omega(\text{Branch}) &= \frac{HW}{p^2} \left(\frac{2}{\gamma^2} p^4 C + \left(2 + \frac{2}{\gamma^2}\right) p^2 C^2 + \frac{29}{\gamma^2} p^2 C + \frac{2}{\gamma^2} p^2 \right) \\ &= \frac{2\gamma^2 + 2}{\gamma^2} HWC^2 + \frac{2p^2 + 29}{\gamma^2} HWC + \frac{2}{\gamma^2} HW \end{aligned} \quad (21)$$

The global branch divides the input into $p \times p$ patches and applied DA among patches, the costs of which are same as equation (21).

Finally, we present the computational costs of DDA as:

$$\begin{aligned} \Omega(\text{DDA}) &= 2\Omega(\text{Branch}) + 2\Omega(\text{Conv}) \\ &= \frac{8\gamma^2 + 4}{\gamma^2} HWC^2 + \frac{4p^2 + 58}{\gamma^2} HWC + \frac{4}{\gamma^2} HW \end{aligned} \quad (22)$$